Spectrochimica Acta Part A: Molecular and Biomolecular Spectroscopy 255 (2021) 119701

Contents lists available at ScienceDirect

Spectrochimica Acta Part A: Molecular and Biomolecular Spectroscopy

journal homepage: www.elsevier.com/locate/saa

Recovered fluorescence of the Cd-nanocluster-Hg(II) system based on experimental results and computational methods

Azarmidokht Sheini [a,1,*], Avat(Arman) Taherpour [1,b,c], Sakineh Farajmand-Amirabadi [1,d], Fatemeh Karampour [e], Maryam Maghsudi [1,d,*], Nadereh Rahbar [d]

[a] Department of Mechanical Engineering, Shohadaye Hoveizeh University of Technology, Susangerd 78986, Iran
[b] Department of Organic Chemistry, Faculty of Chemistry, Razi University, Iran
[c] Medical Biology Research Center, Kermanshah University of Medical Sciences, Kermanshah, Iran
[d] Nanotechnology Research Center, Ahvaz Jundishapur University of Medical Sciences, Ahvaz, Iran
[e] Department of Chemistry Engineering, Faculty of Shariati, Tehran Branch, Technical and Vocational University (TVU), Kermanshah, Iran

HIGHLIGHTS

- Human serum albumin – cadmium nanoclusters (HSA-CdNCs), a label-free off-on fluorescent sensor was synthezied and characterized for Hg^{2+} and biothiols.
- HSA-CdNCs can specifically recognize Hg^{2+} through aggregating NCs and causing fluorescence quenching.
- The calculated limits of detection (LOD) were 55 pM for Hg(II) and 14 nM for GSH, respectively.
- The appropriate molecular mechanics (MM) and quantum mechanical (QM) methods were applied for optimization of the discussed structures of HSA-profile interactions with the Cd-NCs (one atom of Cd), Hg^{2+} and glutathione (G).

GRAPHICAL ABSTRACT

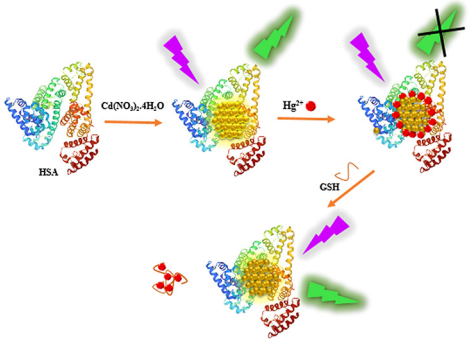

ARTICLE INFO

Article history:
Received 22 December 2020
Received in revised form 23 February 2021
Accepted 9 March 2021
Available online 17 March 2021

Keywords:
Nanoclusters
Human serum albumin
Glutathione
Molecular Mechanics
Quantum Mechanical

ABSTRACT

Human Serum Albumin, a plasma protein existing in abundance, was selected as a template and reducing agent for the formation of CdNCs due to two factors: its stability and low cost. In the presence of human serum albumin (HSA), a selective and sensitive, low-cost, environmental friendly, and label-free off–on fluorescent sensor was synthesized and characterized for a bioaccumulating and toxic heavy metal, Hg^{2+} and biothiols. HSA – CdNCs can specifically recognize Hg^{2+} through aggregating NCs and causing fluorescence quenching. Subsequently, with increase in the concentration of biothiols, Hg^{2+} was eliminated from the surface of NC, while the fluorescence was restored. The calculated limits of detection (LOD) were 55 pM for Hg(II) and 14 nM for GSH, respectively. The assay was capable of detecting Hg^{2+} ions and GHS at different concentrations in the range of 0.008 to 8530 nM and 7.5–5157 nM, respectively. Furthermore, the appropriate molecular mechanics (MM) as well as quantum mechanical (QM) methods were performed to optimize and the theoretical investigation of the discussed HSA-profile structures and its interactions with the Cd-NCs (one atom of Cd), Hg^{2+} and glutathione (G).

* Corresponding authors.
E-mail address: azar.sheini@gmail.com (A. Sheini).
[1] Azarmidokht Sheini, Sakineh Farajmand Amirabadi, Maryam Maghsudi and Avat(Arman) Taherpour, contributed equally to this work in the author's.

https://doi.org/10.1016/j.saa.2021.119701
1386-1425/

1. Introduction

Recently, Photoluminescence (PL) probes have been reported to be turned-off/on in the presence of heavy metal ion (HMI) (such as Hg^{2+}) and chelators such as cellular thiol compounds [1]. This is while the rise in HMI contamination has raised concerns. Therefore, it is highly important to develop fast, cheap, selective, and sensitive fluorescent sensors for heavy metals considered as dangerous, namely Cd, Hg, and Pb [2]. In case their exposition to the mentioned elements exceeds a certain limit, they can signal the potential of having serious pernicious impacts on the environment, more specifically on human health [3].

Mercury can cause detriments to the people's nervous system even if it exists in parts per million (ppm) concentration. It is also a major threat to both the human health and environment because of its potentiality of being accumulated in ecological systems [1]. Further, it has been identified as an environmental pollutant for several decades. Despite being recognized as highly toxic in all its oxidation case, mercury reveals variation in solubility and possible redox interconversion [4]. Mercury poisoning induces myriad detrimental human diseases, including brain damage [5], kidney inefficiency, and various cognition and motion disorders [6]. In this line, The United States Environmental Protection Agency (US EPA) has ordered national regulations for the maximum pollutant level of mercury in drinking water to be 2 ppb, which, according to the regulations, has no pernicious health effects [7].

Besides, glutathione (GSH, L-γ-glutamyl-L-cysteinylglycine known as an endogenous detoxicant) has water solubility, stable activity, and ease of availability; it is a tripeptide composed of glutamic acid, cysteine, and glycine which can easily coordinate with various components, including medicines, toxins, and toxic heavy metal ions [8]. Noteworthy, GSH is the most abundant cellular thiol compound that plays a significant role in combating against stress resulted from oxidation in cells [9]. Abnormal levels of GSH have a direct relationship with various types of diseases, including but not limited to cancer, AIDS, Alzheimer's, and cardiovascular diseases [10]. Given these characteristics, it is desirable to develop a simple and low-cost strategy for a selective and sensitive diagnosis of biothiol in the biological sample in the primary clinical diagnosis of these diseases; it is also important to monitor the potential toxic Hg^{2+} metal in aquatic ecosystems.

Among variously reported PL probes, the label-free strategy has shown obvious advantages [2,3]. This method does not urge dual labelling or pre-tagging of biomolecules، which is usually an unconventional task requiring expensive equipment and time-consuming sample preparation [11,12] Metal nanoclusters are of sub-nanometer sizes which have manifested size-dependent optical and magnetic properties [13]. M−NCs have a cost-effective synthesis, besides being photostable, of fluorescent nature and biocompatible, hence they are incrementally used in various chemosensors, biological imaging, catalysis, and environmental and electronic devices [14]. Many synthetic methods have been reported to produce metal nanoclusters. Over the past few years, a wide range of studies have been conducted on the synthesis of luminescent M−NCs in the presence of various reducing agents, such as protein [15], peptides [16], DNA [17], thiols [18], dendrimer [19] and polymer [20].

Among these methods, NC synthesis of protein templates has manifested many advantages as far as biological applications are concerned. The protein-directed synthesis methods render significant merits, including being simple, non-toxic and much friendly regarding environmental impacts [21].

Based on the foregoing reasons and previous studies, PL probes containing the functional groups of N, S, and O can facilitate chelation with metal ions, lead to efficient quenching [22], and be restored by chelators; accordingly, human serum albumin (HSA) (as the sulfur, nitrogen, and oxygen source) was selected for the synthesis of CdNCs. The selected synthesis method is very straightforward, besides having the potential of being performed in "one-pot" fashion under mild conditions. In this study, conducting a straightforward as well as green chemical method, water-soluble CdNCs with low toxicity and good stability were synthesized (Scheme 1). In a nutshell, highly fluorescent CdNCs were synthesized, characterized, and further developed as an ultrasensitive sensor of Hg^{2+} and biothiols. In this study, the optimization of the discussed structures by the appropriate MM and QM methods were also performed to discuss the experimental results. The results were evaluated to demonstrate the interactions of HSA and glutathione (G) with Hg^{2+} ion and Cd in HSA-Cd-NCs, HSA-Hg^{2+} and G. The obtained results were applied to compare the stabilities of HgG2 and the species after removing Hg^{2+} from profile-HSA-Hg^{2+} structure.

2. Experimental

2.1. Reagents

All Metal salts were prepared from Merck (Darmstadt, Germany). L-glutathione (GSH), Human Serum Albumin (HSA, lyophilized powder ≥ 96%), and all amino acids were purchased from Sigma-Aldrich. All reagents with the degree of analysis were employed, without any further purification.

2.2. Synthesis of bovine serum Albumin-Capped CdNCs (BSA–CdNCs)

HSA-stabilized Cd nanoclusters were synthesized by the reaction of Cd(NO3)2·4H2O (5 mL, 7 mM) with HSA solution (5 mL, 10 mg/mL) with stirring at room temperature. After 3–5 min, the NaOH solution was added to adjust pH to the pH 12. Finally, after several hours (typically 24 h) of stirring at 50 °C, a yellow solution of HSA-CdNCs was centrifuged (12000 rpm, 15 min) and then dialyzed for 24 h against PBS buffer using a dialysis tubing (MW = 12 kDa) for characterization. The resulted solution was kept at 4 °C for subsequent tests. To obtain desirable HSA-CdNCs, pH, Cd concentration, temperature, and counter ion were controlled.

2.3. Apparatus

Analysis of Transmission Electron Microscopy (TEM) and dynamic light scattering was done by a Philips CM30 transmission electron microscope (voltage of 200 KV) and Zetasizer Nano ZS instrument (Malvern Instruments Ltd., Malvern, Worcestershire, UK), respectively. Also, JASCO spectrofluorimeter (FP 6200), a Bruker ALPHA, UV-Win T80 spectrophotometer and JASCO J-810 spectropolarimeter were used for fluorescence, FT-IR spectra, UV–Vis and circular dichroism (CD) measurements, respectively.

2.4. Signal-off –on assay of Hg2+ ions and GHS

To estimate the sensitivity to Hg2+, different concentrations of Hg2+ solution were added to an aliquot of HSA-CdNCs (200 μL, in phosphate-buffered saline (PBS,10 mM, pH 7.4, 1.8 mL) and titrated by consecutive additions of Hg2+ solution (0.005–6976 nM). The combination was then allowed to react at room temperature for 2 min. Fluorescence intensities were followed by being measured at an emission range of 400–700 nm with λex 390 nm (slit width; excitation: 5 nm; emission: 10 nm). The LOD and linear detection range of Hg2+ were specified. To specify the relative selectivity of HSA-CdNCs towards Hg2+, interference studies were conducted on certain common heavy metal ions.

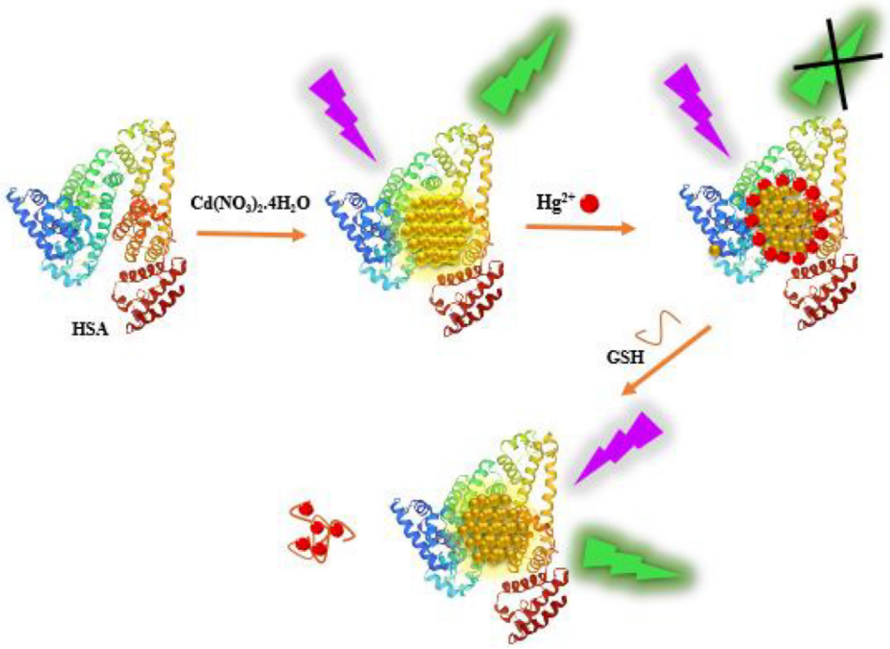

Scheme 1. Schematic representation of off / on sensor based on the CdNCs.

Different concentrations of GHS were added to the HSA-CdNCs/Hg2 + system and incubated for 10 min at room temperature. Afterwards, the fluorescence spectra were done by employing a 390 nm excitation wavelength. In order to witness any possibility of presence of other amino acids, a similar procedure was followed.

2.5. Detecting Hg^{2+} in real samples

Tap (from our laboratory and from Ahvaz Jundishapur University of Medical Sciences, Iran) and Karun River water samples were collected following their filtration with a 0.45 μm micropore membrane. The water samples were spiked with different concentrations of Hg^{2+} ions and incubated for 10 min at room temperature. Afterwards, the fluorescence spectra were done by employing a 390 nm excitation wavelength.

3. Results

3.1. Synthesis and characterization of fluorescent CdNCs

Biomolecules have gained significant attention as efficient in reducing and stabilizing agents for the synthesis of MNPs primarily owing to their biocompatibility, good water solubility, richness in functional groups (such as thiol, hydroxyl, carboxyl, and amine) and ease of further bioconjugation [23]. Biomolecules such as human albumin serum and bovine serum are efficient etchants for the synthesis of metal NC due to having disulfide bonds and a free thiol group provided by cysteine (Cys34) [23,24]. In the presence of protein as a reducing and stabilizing agent, metal ion–protein adducts were formed and then with increasing pH, metal ions decreased [25,26].

3.2. Optimizing the conditions of experiment for the synthesis of HSA-CdNCs.

HSA, a ligand with the basis of multi-functionality, was selected as both a reducing agent and a capping agent in alkaline medium for the synthesis of CdNCs. To optimize the synthesis, the effects of salt type and concentration, solution pH, and temperature were investigated on the fluorescence intensity of the as-synthesized HSA-CdNCs, and the optimal values of these parameters were further specified.

Temperatures ranging from 25 to 55 °C were selected. The fluorescence intensity of the HSA – CdNCs exceeded above 55 °C (data not shown). That being said, since HSA has the quality of being denatured at higher temperatures, the limit for temperature was set at 55 °C.

Second, the reaction pH, as an important factor, was considered for fluorescence sensor systems. As observed in Fig. 1a, at pHs less than 8, HSA did not have a reducing ability to form CdNCs, and the intensity of the fluorescence emission was very weak. With increasing the solution pH (pH 10), white precipitation of Cd(OH)2 was formed. With further increase in the solution pH (>10), the reduction capability of HSA was activated. As the reaction proceeded at pH 12, the solution gradually turned into a clear solution, indicating the dissolution of Cd(OH)2 and the formation of CdNCs. The possible mechanism for HSA templated synthesis of CdNCs was in accordance with literature procedure [27]. We hypothesized that the high pH could activate the sulfide groups for reacting with the Cd ions of BSA. That being said, an optimal pH of 12 was regarded for extra tests.

Another considerable factor was the concentration ratio of Cd to HSA (Fig. 1b). As can be seen, the cluster formation began at a Cd:HSA molar ratio of 10:3 with 480 nm emission band, and then increased and shifted to 500 nm with the increase in Cd:HSA ratio. The highest fluorescence intensity for HSA – CdNCs was achieved at Cd: HSA molar ratio of 70:3. With further increase in the Cd:HSA ratio (100:3), the fluorescence intensity of HSA – CdNCs decreased. Therefore, a Cd: HSA molar ratio of 70:3 was chosen.

Ultimately, the influence of salt type was further considered. Based on the results, the emission of NCs depended on the salt type, and the most intense fluorescence was achieved for cadmium nitrate. The emission spectrum of CdNCs excited at 390 nm and emitted at 500 nm under optimized conditions including pH 12,

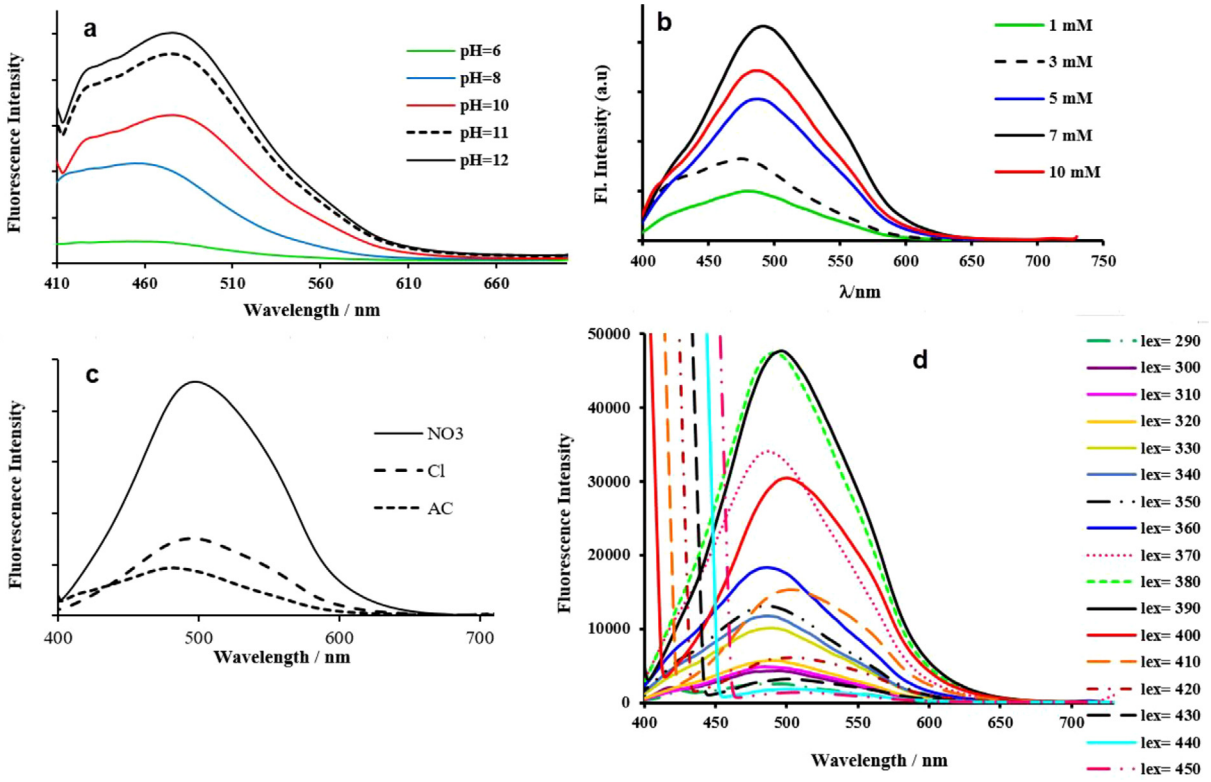

Fig. 1. Photoluminescence spectra (λex = 390 nm) of HSA – CdNCs synthesized a) at different pHs, b) in different concentrations of Cd ion while keeping the HSA concentration constant, i.e. 20 mg/mL. The final metal ion concentrations are 1, 3, 5, 7 and 10 mM. Results indicate that emission of NCs depends on the metal ion to BSA concentration ratio, and the most intense fluorescence was obtained in Cd:BSA molar ratio of 50:3, c) the effects of salt type, d) Emission spectra of HSA – CdNCs (from 290 to 450 nm, in 10 nm step size.

Cd: HSA molar ratio of 70:3, 50 °C, and 24 h incubation (Fig. 1c). Next, the synthesized HSA – CdNCs was characterized by applying UV–Vis absorption, FT-IR, fluorescence and circular dichroism (CD) spectroscopy, DLS, and TEM imaging.

Fig. 1d demonstrates the fluorescence spectra of the HSA – CdNCs at 500 nm with the excitation wavelengths between 290 nm and 450 nm. The emission intensity at 500 nm grew in the excitation range of 290–390 nm and then gradually decreased. However, the maximum emission peak at 500 nm was detected independent of the excitation wavelength range.

To confirm the in situ formation of HSA – CdNCs, UV–vis absorption spectroscopy was also employed. Fig. 2a shows the absorption spectra of HSA – CdNCs and native HSA. Compared to pure HSA, the reduction in the absorption band at 285 nm was related to the change in the phenylalanine, tyrosine (Tyr) and tryptophan (Trp) residues structures that had a role in the reduction of the Cd ions [28]. The emergence of the adsorption band at 350 nm confirmed CdNCs formation.

Circular dichroism (CD) and FT-IR spectroscopy were employed to study the secondary/tertiary structures of proteins.

Circular dichroism (CD) spectroscopy is considered as one of the most economical methods for investigating the conformational alterations of HSA followingHSA – CdNCs nucleation [29]. Given the effect of HSA – CdNCs on the HSA secondary structure, CD spectra of HSA were determined in the absence and presence of CdNCs. The characteristic bands of α-helix structure at 208 and 222 nm were indicated in the protein control samples (Fig. 2b, curve in black) [30]. The CD spectra of HSA – CdNCs showed a remarkable increase in the negative ellipticity at 208 nm with a concomitant decrease in the negative ellipticity at 222 nm; both bands also shifted towards lower wavelengths [31]. The change in α-helical was the result of (1) alkali denaturation (2) formation of Cd - groups (N, O, OH, and NH2) bond, and (3) agglomeration at 50 °C. Changes in the secondary and tertiary structures of the protein may also be due to cleavage of disulfide bonds and formation of Cd-S bonds [15,32].

Another common approach to specifying the alteration in the secondary structure of the protein (amide bands) could be confirmed by Infrared spectroscopy (FTIR) [33]

The characteristic bands of native HSA at C═O stretching (1700–1600 cm^{-1}), N—H bending and C—N stretching (1620–1500 cm^{-1}) and the blending of C—N stretching, in-plane C═O bending, and C—C stretching (1229–1,301 cm^{-1}) are related amides I, II and III, respectively. The band at 3400–3,000 cm^{-1} are assigned to N—H and O—H stretching vibrations [26]. Compared to the FTIR spectra of native HSA, the disappearance of the band at 3290 cm^{-1}, the bands of amide I at 1652 cm^{-1} and amide II at 1540 cm^{-1} and appearance of a single intermediate strong peak at 1640 cm^{-1} with a shoulder of at 1518 cm^{-1} indicated Cd-NCs formation (Fig. 2c, curve in black). These changes can be attributed to (1) the interaction of the metal surface with the N—H functional groups [34] and [2] the excessive surface water in the FT-IR spectra of wet HSA – CdNCs [35].

The decrease and changes in the positions, shapes, and intensities of these bands reflect alterations in the secondary structure of HSA, the binding of Cd to —NH_2 and —COOH, and facilitation of the NCs. The above results reveal that the highly basic condition promoted interaction between HSA and metal ion besides the conformational change of HSA [36,37]. The FT-IR results further corroborated the findings of CD spectroscopy, firmly suggesting a remarkable conformational change in the structure of protein with the formation of the HSA – CdNCs [38,39]. This finding is in agreement with the observation having been reported earlier by others concerned with the issue [40,41].

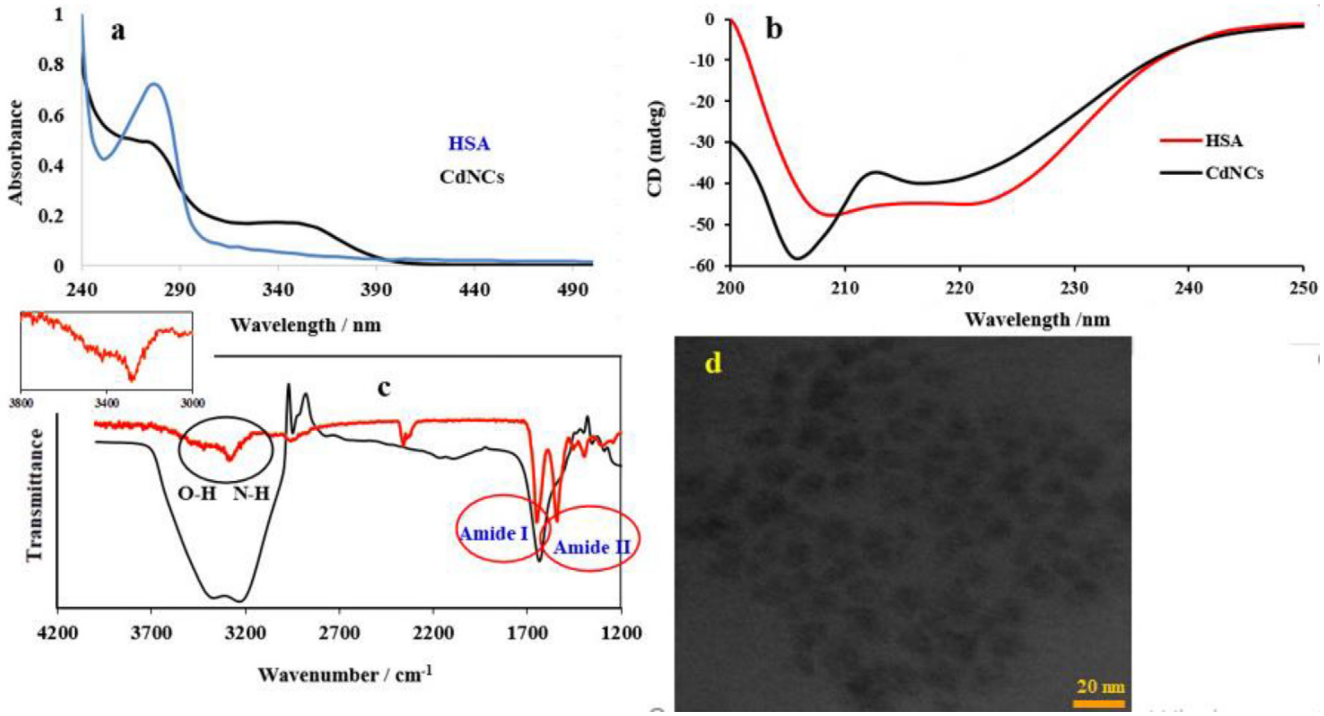

Fig. 2. UV–vis absorption spectra of free HSA and CdNCs, (c) CD spectra of free HSA and CdNCs, (c) FT-IR spectra of free HSA (1) and CdNC (d) TEM image of CdNCs.

TEM was performed to determine the size and morphology of t HSA – CdNCs. As shown in Fig. 2d, the HSA – CdNCs were nearly globular, uniform, and optimally-isolated in the range of 2–8 nm with an average diameter of around 5 nm. The hydrodynamic radius of CdNCs was specified by DLS to be 10 ± 0.5 nm (Fig. 2e), which seems to be larger than the radius measured by TEM.

To test the performance of this fluorescent probe, the HSA – CdNCs was used to detect Hg^{2+} and GHS.

3.3. Fluorescence turn-off detection of Hg^{2+} ions

To study the feasibility of fluorescence, the response of the sensors towards different Hg^{2+} concentrations was measured. Based on Fig. 3a, the PL intensity of the HSA – CdNCs was sensitive to Hg^{2+} concentration and fluorescence remarkably decreased within 2 min following the addition of Hg^{2+} ions. This implies the potentiality of the application of HSA – CdNCs as an extremely sensitive "turn-off" fluorescence probe for Hg^{2+} ion. As it can be observed in Fig. 3b, the plot of (F_0/F) versus [Hg^{2+}] indicates one excellent linear correlation graph with correlation coefficients (R^2) of 0.9977, over mercury concentrations of 0.008–0.1 nM. The LOD was obtained (54 pM, S/N = 3), which seems to be extremely less than the safe limit of Hg^{2+} ions in drinking water (i.e., 2 ppb, ~10 nM) brought about by the U.S. EPA) [42]. Table 1 displays, through comparison, the sensing performance of different fluorescent probes for Hg^{2+}. According to this table, our sensing system manifested much sensitivity over the up-to-date reported sensing systems. Another essential parameter for assessing the performance of sensing system is selectivity. To evaluate the selectivity of HSA – CdNCs, the interference effects of 22 different cations were explored under optimal conditions. Compared to 6 μM of Hg^{2+}, HSA – CdNCs probe had only a negligible fluorescence quenching effect following the addition of 100 μM of K^+, Na^+, Mg^{2+}, Ca^{2+}, Cu^{2+}, Ni^{2+}, Zn^{2+}, Pb^{2+}, Fe^{2+} and Fe^{3+} ions (Fig. 3c).

The results for determination of Hg^{2+} in real samples are summarized in Table 2. As it can also see from Table 2, the results imply that our method has satisfactory potential for quantitative analysis of Hg^{2+} in real samples.

According to similar mechanisms described regarding the synthesis of AuNCs, increase in the pH > 10 (the pK_a of Tyr) causes formation of Cd0 atoms [42]. Further, decrease in fluorescence intensity can be ascribed to (1) the d10–d10 metallophilic interaction of Cd0 (4d10) and Hg^{2+} (4f145d10), (2) the interaction between the HSA shell of the cluster and Hg^{2+} ions leding to the NCs aggregation, or (3) the interaction between Hg (soft donor) and sulfur atom (soft acceptor) [43].

To investigate NCs aggregation in the presence of Hg^{2+}, DLS images of HSA – CdNCs (Fig. 4a, curve in red, average size of 10 ± 0.6 nm) and CdNCs/Hg^{2+} (Fig. 4a curve in black, size of 15–30 nm), were taken. According to DLS results, theluminescence quenching could be attributed to second mechanism. We propose that the presence of the NCs aggregation also played a significant role in the fluorescence detection process. The luminescence recovery of the HSA – CdNCs /Hg^{2+} in the presence of GHS is due to the GHS– Hg^{2+} complex formation which can confirm the mechanism of aggregation thus, third mechanism is rejected [15,44].

3.4. Signal-on fluorescence detection of GHS

Hg^{2+} ions showed high affinity to Thiol-containing GSH, which could restore the quenched PL emission of HSA-CdNCs – Hg^{2+} system. Turn/on sensor can be applied in both the selective and sensitive processes of detecting GSH. Obviously, with the increase of GSH, the PL was restored and subsequently the intensity of the emission increased, resulting in the release of Hg^{2+} from the surface of HSA – CdNCs with the formation of strong Hg^{2+}-S or Hg^{2+}–NH bonds (Fig. 4b). The insets of Fig. 4c exhibited a good linear relationship between F_0/F and the concentration of GSH from 7.5 to 372 nM (R^2 0.9993). The calculated LOD was 14 nM, which was significantly less than those of the previously-mentioned fluorescence probes (Table 1). To assess the selectivity of the present biosensor system, the sensor response to other amino acids (Ala, Arg, Glu, Gly, His, Lys, Ser, Thr, Cys, Hcy and Tyr) was further exam-

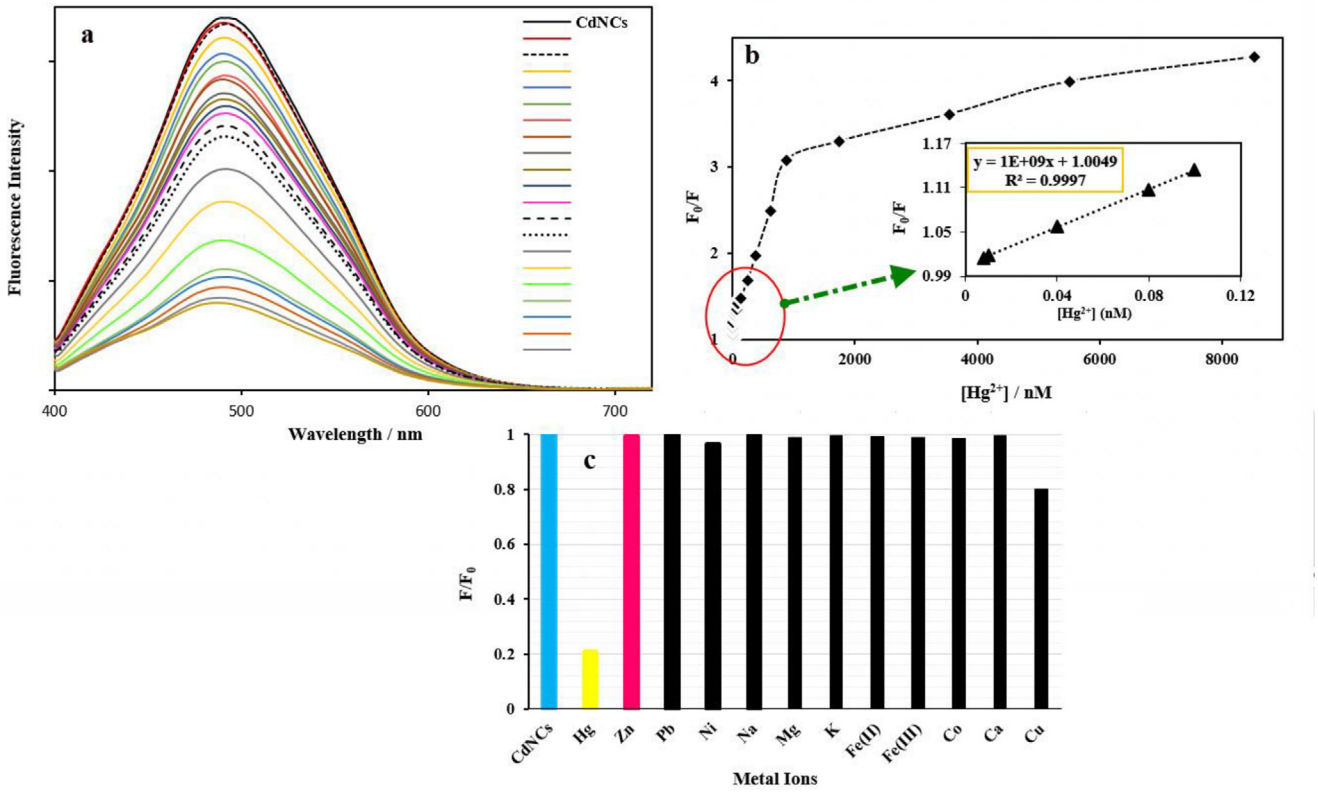

Fig. 3. a) Fluorescence spectra of HSA – CdNCs with increasing of Hg^{2+} b) plots of (F_0/F) versus concentrations of Hg^{2+}, Inset indicates the linear range from 0.008 to 0.1 nM, c) Fluorescence response in the presence of concentration of different cations.

Table 1
Comparison of the analytical characteristics of HSA-CdNCs probe with some reported fluorescent probes for specific detection of Hg^{2+} ion and glutathione in different samples.

	DLR[1]	LOD[2]	Ref.
Probe-Hg^{2+}			
CCYR6H4-AuNCs		30 nM	[42]
dBSA Ag clusters	10 nM-5 μM	10 nM	[43]
L-cys/CS-AuNC	0–1000 nM	3 nM	
CDs/AuNCs@ZIF-8	3–30 nM	1 nM	[44]
Carbon quantum dots (CQD) - f-MWCNTs)	1–12 nM	0.5 nM	[45]
Copper nanoclusters/carbon nitride nanocomposite	0.5–10 nM	0.01 nM	[46]
Fibrinogen- gold Nanocluster ((FBG-AuNCs)		150 nM	[47]
HSA – CdNC	0.008 to 8530 nM	55 pM	This Work
Probe-GHS-Hg^{2+}			
GO-Ru complex	0–6.0 μM (Hg) 0.0–5.0 μM (GHS)	2.34 nM (Hg) 4.6 nM (GHS)	[48]
Probe-GHS			
ZnS quantum dots	2–10^4 μM	0.9 μM	[49]
Metal-organic framework (MOF) (UiO-67-sbdc)	0.5–10 mM	97.5 μM	[50]
Albumin-stabilized gold nanoclusters	10–400 μM	1.2 μM	[51]
PSDs/Ag		74.9 nM	[52]
Gold-copper metal–organic framework	1–10 μM	0.3 μM	[53]
CDs@ZIF-8 nanocomposites	10 to 300 μM.	1.04 μM	[54]
HSA – CdNC	7.5–5157 nM	14 nM	This Work

[1] DLR dynamic linear range, [2]LOD limit of detection.

ined. As it has been shown in Fig. 4d, the assay responses were not affected by the interfering species such as amino acids, implying that amino acids had no competing reaction with GSH. The effectiveness of HSA – CdNCs, as a sensor for the determination of Hg^{2+} and GSH was compared to the findings of the previously-published works, the results of which listed in Table 1. In this regard, HSA – CdNCs was able to monitor Hg^{2+} and GSH with high selectivity and sensitivity. Fig. 4c depicts the formation of HSA – CdNCs and its binding with both Hg^{2+} and GSH.

3.5. Computational methods and modelling details

The optimization of the discussed structures was performed by appropriate molecular mechanics (MM) and quantum mechanical (QM) methods. The results were interpreted based on the best results of the optimization and minimization of the structures [55,56]. The molecular mechanics MMFF94, UHF-PM6 and DFT-B3LYP/6-31G* (and LANL2DZ > Kr) methods were done by the Spartan'10 package [55].

In Fig. 5, the modelled diagram of HSA-profile interactions with the Cd-NCs (one atom of Cd), Hg^{2+} and glutathione (G) on the basis of the experimental section has been demonstrated. The selected profile of HSA includes –Glu-Lys-Cys-Cys-Lys-Ala-Asp-Asp-Lys-Glu-Thr-Cys-Phe-Ala-Glu- amino acids [57]. It is noticeable to add that the processes of interactions of Cys amino acids (in the selected profile) with Cd-NCs and Hg^{2+} have been investigated in the experimental section. As it could be seen in Fig. 5, the HSA-profile first interacts with Cd-NCs and Hg^{2+}, then G interacts with Hg^{2+} of HSA-Hg^{2+}. In what follows, the related energy levels will be discussed.

The modelled structure of the profile of HSA, HOMO and LUMO energy levels, HOMO-LUMO energy gap and its equivalent wavelength have been depicted (Fig. 6). The HOMO-LUMO energy gap

Table 2
Results of recovery studies from Tap and Karun River water samples spiked with Hg2 + ions by HSA – CdNCs.

Sample	Spiked amount (nM)	Found amount (nM)	Recovery (%)	RSD
Tap water				
1	**10**[a]	**9.83**	**98.3**	**2.2**
2	**20**	**19.8**	**99**	**1.9**
Karun River water				
1	**10**	**9.65**	**96.5**	**2.3**
2	**20**	**19.7**	**98.5**	**2.1**

[a] Each value is the average of 3 replicate measurements.

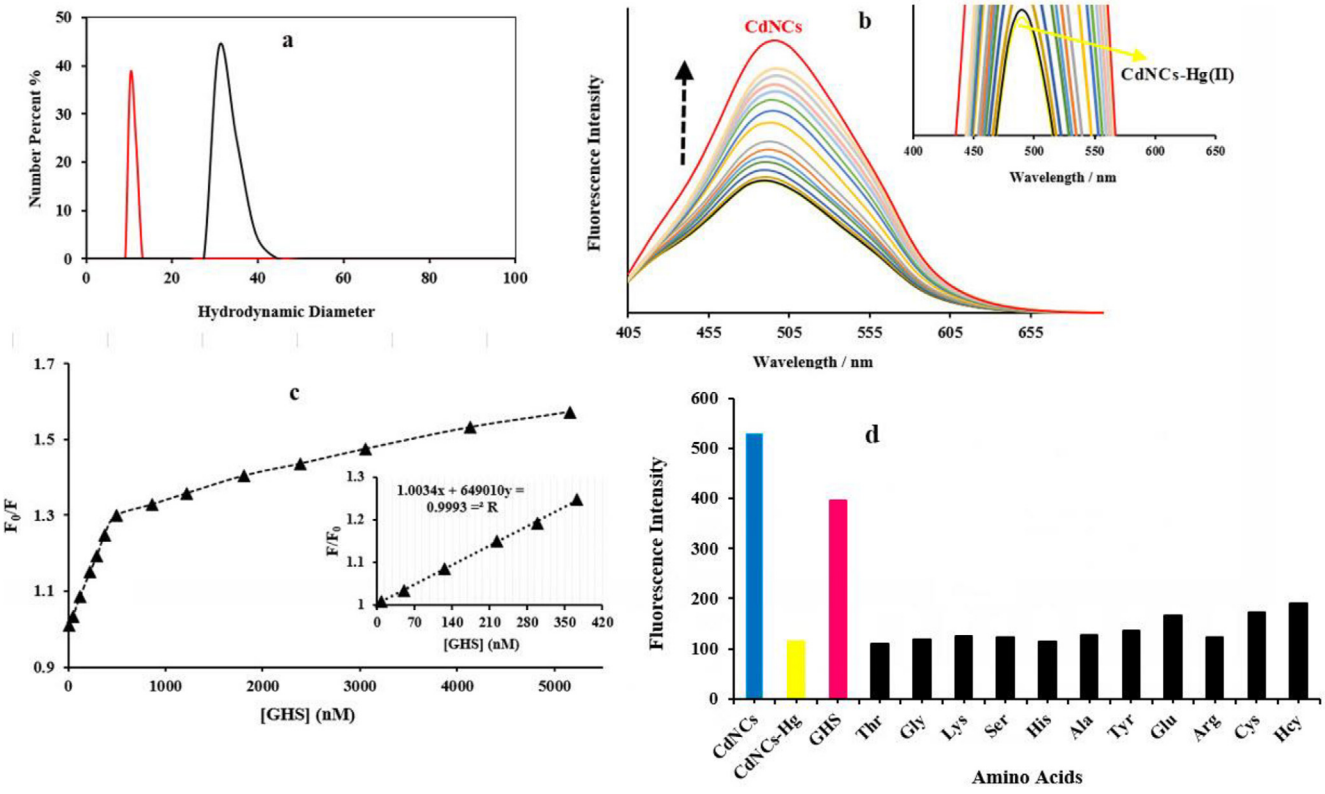

Fig. 4. a) Fluorescence spectra of HSA – CdNCs containing Hg^{2+} with addition of GHS at 500 nm (λex = 390 nm). b) plot of (F/F_0) versus GHS concentration, c) Fluorescence response in the presence of concentration of different amino acids.

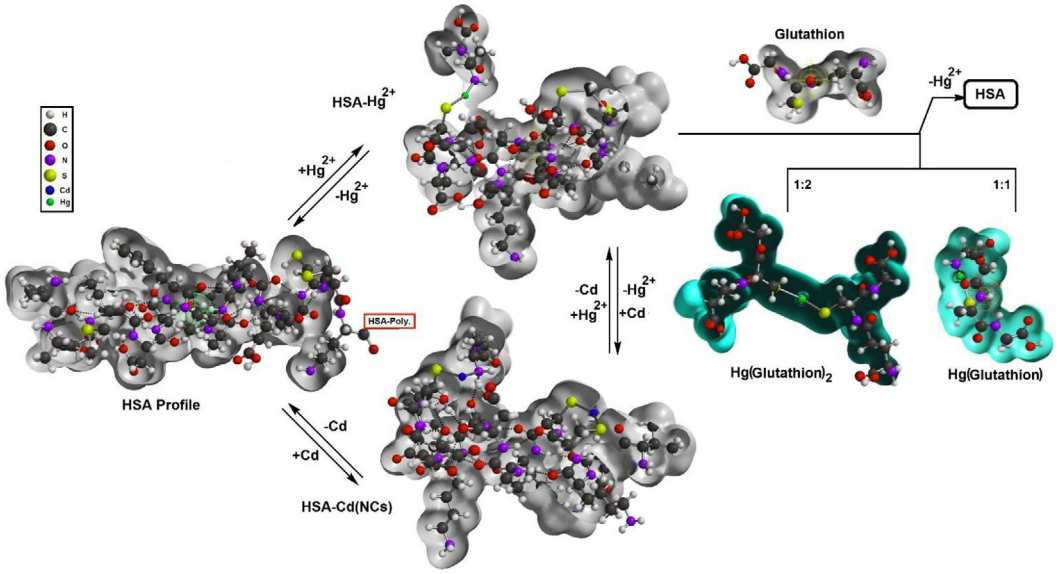

Fig. 5. The modelled diagram of HSA-profile interactions with the Cd-NCs (one atom of Cd), Hg^{2+} and glutathione (G) on the basis of the experimental section.

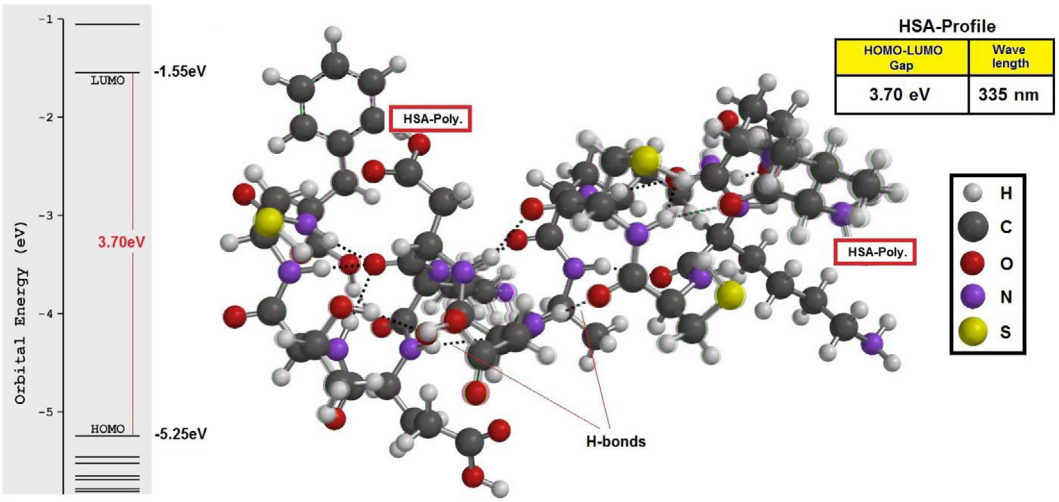

Fig. 6. The modelled structure of the profile of HSA, HOMO and LUMO energy levels, HOMO-LUMO energy gap (3.70 eV) and its equivalent wavelength (335 nm).

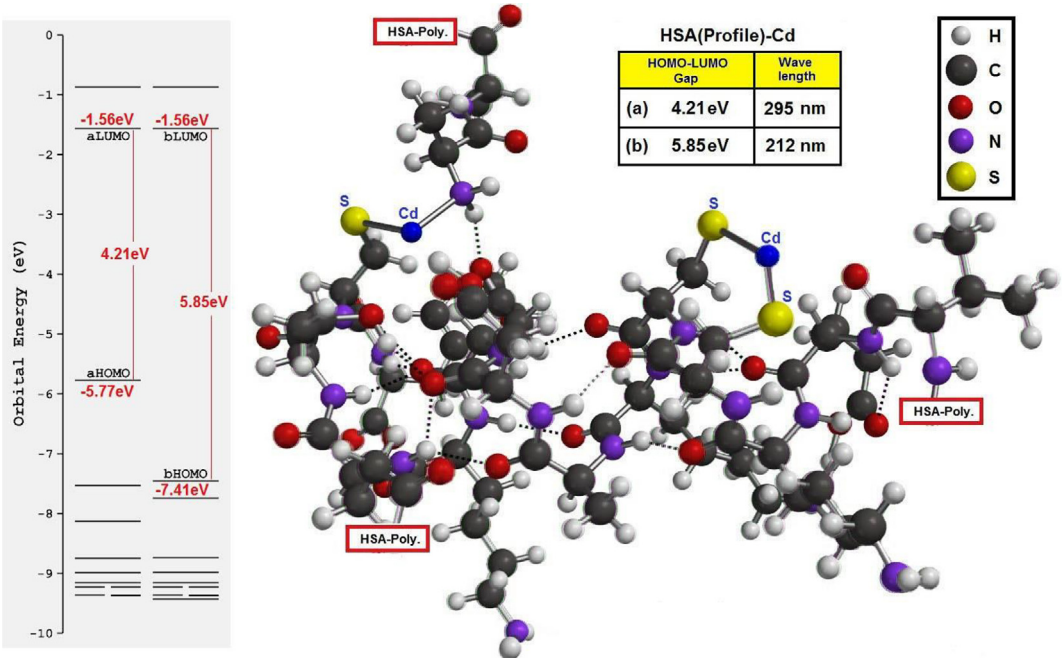

Fig. 7. The modelled structure of the profile of HSA-Cd-NCs, HOMO (a & b) and LUMO (a & b) energy levels, HOMO-LUMO energy gaps (4.21 and 5.85 eV) and its equivalent wave length (295 and 212 nm), respectively.

of the selected HSA-profile was calculated to be 3.70 eV. This amount of ΔEHOMO-LUMO (in eV) is equal to 335 nm of UV wavelength.

The modelled structure of the profile of HSA-Cd-NCs, HOMO(a), HOMO(b), LUMO(a), LUMO(b) energy levels, HOMO-LUMO energy gaps (ΔEHOMO-LUMO (a & b) in eV) was also displayed. The ΔE HOMO-LUMO(a) and ΔE HOMO-LUMO(b) of profile-HSA- Cd-NCs were computed and recorded as 4.21 and 5.85 eV, respectively (Fig. 7). The obtained results are equivalent to the UV wavelength 295 and 212 nm, respectively.

The modelled structure of the profile of HSA-Hg^{2+}, HOMO and LUMO energy level, HOMO-LUMO energy gap and its equivalent wavelength have been demonstrated. The HOMO-LUMO energy gap of the selected HSA-profile was calculated to be 5.16 ev (Fig. 8). This amount of ΔE HOMO-LUMO (in eV) is equal to 240 nm of UV wavelength. So, the interaction between profile-HSA with Cd-NCs results in change in ΔEHOMO-LUMO from 3.70 eV (in profile-HSA) to 4.21 eV (in HOMO-LUMO (a) of the profile-HSA-Cd-NCs. It means that the UV wavelength underwent change, a reduction from 335 nm (in profile-HSA) to 295 nm (in profile-HSA- Cd-NCs, See Figs. 6 and 7. The interaction between Hg^{2+} with the profile- HSA- Cd-NCs leads to alteration in ΔEHOMO-LUMO(a) from 4.21 eV (in profile- HSA- Cd-NCs to 5.16 eV (in profile-HSA-Hg^{2+}). It means that the UV wavelength reduces from 295 nm (in profile-HSA) to 240 nm (in profile-HSA-Cd-NCs), See Figs. 7 and 8.

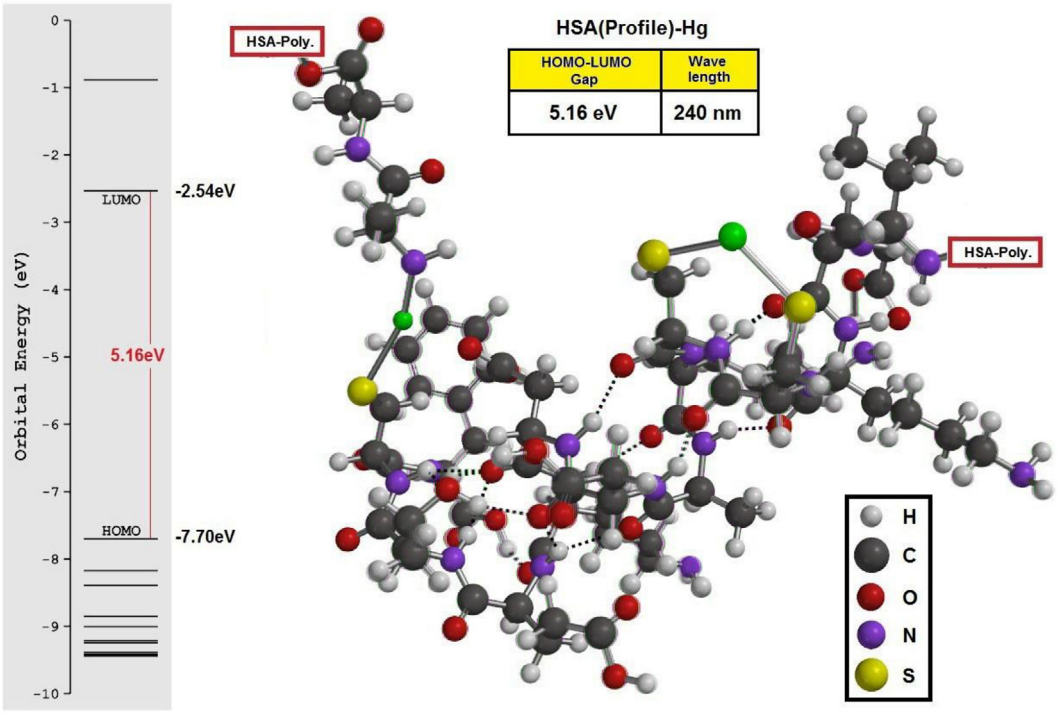

Fig. 8. The modelled structure of the profile of HSA-Hg^{2+}, HOMO and LUMO energy level, HOMO-LUMO energy gap (5.16 eV) and its equivalent wave length (240 nm).

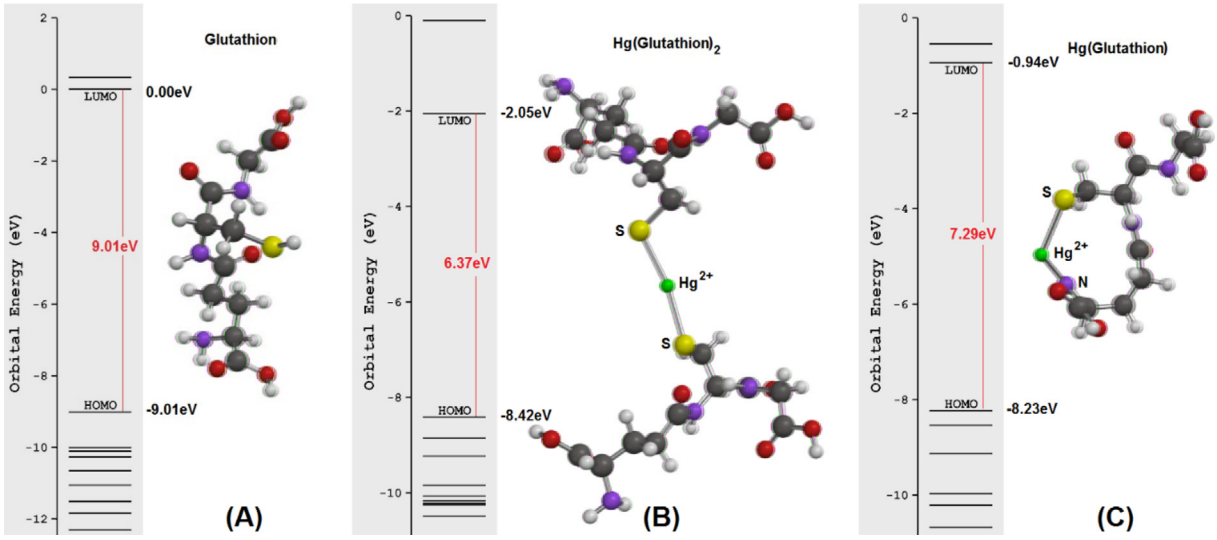

Fig. 9. The modelled structure of the profile of G (A), HgG2 (B), HgG (C), their HOMO and LUMO energy levels and HOMO-LUMO energy gaps.

The modelled structure of the profile of G, HgG2, HgG, their HOMO and LUMO energy levels and HOMO-LUMO energy gaps have been displayed in Fig. 9(A–C). The HOMO-LUMO energy gaps (ΔEHOMO-LUMO) of G, HgG2 (1:2 ratio) and HgG (1:1 ratio) were calculated to be 9.01, 6.37 and 7.29 eV, respectively. The results of the calculations following the energy-mass balance demonstrated that HgG2 (with 1:2 ratio) 40 kcal.mol^{-1} was stable than HgG (with 1:1 ratio). Moreover, ΔEHOMO-LUMO of HgG2 (1:2 ratio) was 0.92 eV lower than HgG (1:1 ratio). This signifies the stability of HgG2 in comparison to HgG. As a consequence, not only HgG2 is the one species that may be constructed in the Hg^{2+} with G, but also its reactivity is more than HgG. The complex of HgG2 could be obtained when G acts with the profile-HSA-Hg^{2+}.

The energy diagrams of the HSA-profile interactions with Cd-NCs and Hg^{2+} (Fig. 10A) have been depicted. Also the energy diagrams of the glutathione process with HSA-Hg^{2+} to produce HgG2 have been shown (Fig. 10B). All the results were obtained following the "energy-mass" balances. The results of the calculations indicated that the HSA profile with Cd-NCs has made profile-HSA-Cd-NCs, which was assessed to be 55.57 kcal.mol^{-1} more stable than HSA + Cd-NCs. This is while the profile-HSA-Hg^{2+} with 81.33 kcal.mol^{-1} was more stable than HSA + Hg^{2+}. See Fig. 10(A). The results after energy-mass balance and evaluation demonstrated that profile-HSA-Hg^{2+} was 26.76 kcal.mol^{-1} more stable than profile-HSA-Cd-NCs. Also, the willingness of interaction between Hg^{2+} with the profile of HSA and profile-HSA-Cd-NCs has

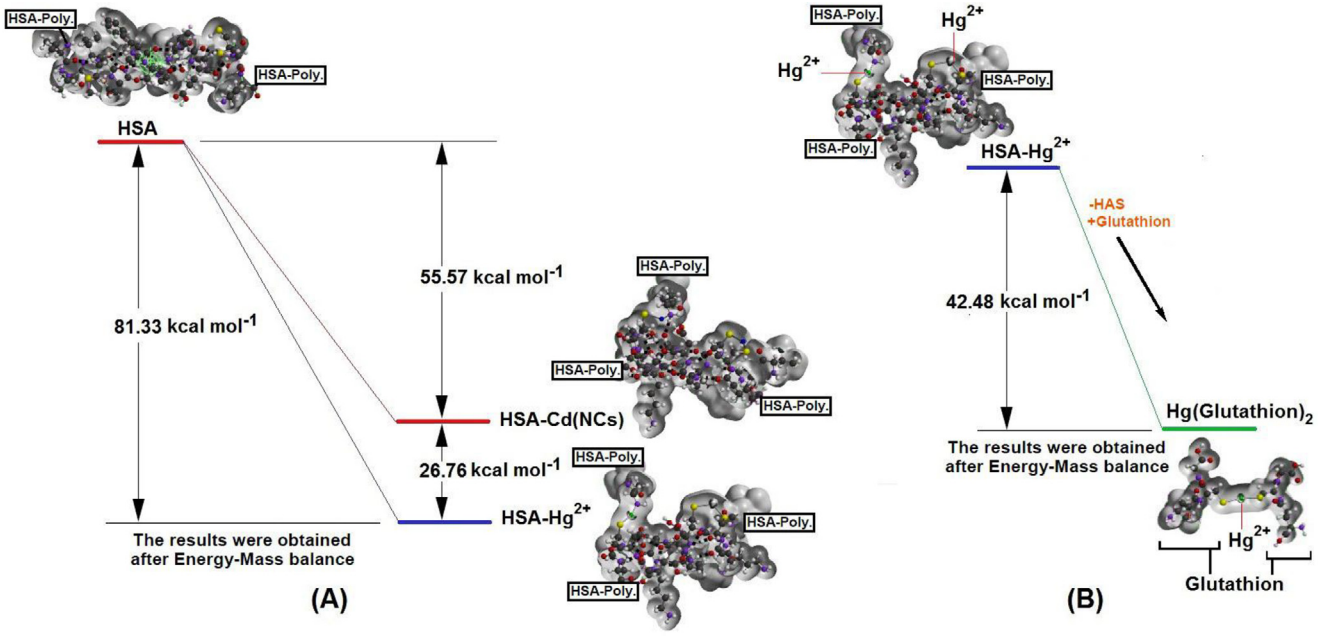

Fig. 10. (A) The energy diagrams of the HSA-profile interactions with Cd-NCs and Hg^{2+}, (B) The energy diagrams of the glutathione process with HSA-Hg^{2+} to produce HgG2. All the results were obtained after "energy-mass" balances.

been shown. Also, the obtained results after "energy-mass" balances demonstrated that HgG2 takes 42.48 kcal.mol^{-1} stability in comparison with the appropriate species following the removal of Hg^{2+} from profile-HSA-Hg^{2+} structure.

4. Conclusion

Ions of Hg^{2+} are widely dispersed in soil and water, hence able to easily enter the human body through the food chain. Furthermore, abnormal levels of GSH exhibit relationships with different diseases. It is necessary to develop a biosensor for sensing intracellular GHS and Hg^{2+}. A simple sensing on – off platform for Hg^{2+} and GHS detection was reported based on an S-rich HSA. The HSA – CdNCs fluorescent probe in the present project detected Hg^{2+} and GSH based on the accumulation of NCs and the interaction of Hg^{2+} of HSA-CdNCs – Hg^{2+} system with – S or N— H of GSH, respectively. This assay offers multiple considerable advantages: first, it is simple and cost-effective and has a one-step design, providing a suitable protocol for a rapid detection of Hg^{2+} and GSH against other metal ions and natural amino acids with low LODs of 54 pM and 14 nM, respectively. Second, further bioconjugation for HSA – CdNCs is required. Finally, the proposed assay showed a good linear range for both and low-level detection limit (GHS (14 nM), Hg^{2+} (54 pM)) compared to the previous methods. Furthermore, it seems that this sensor may offer low-cost, sensitive sensors, besides novel method with high affinity to Hg^{2+} ions and GSH in the presence of other co-existing compounds which can ultimately lead to detecting the low concentration of both in aqueous samples. The optimization of the discussed structures was performed by the appropriate MM and QM methods to interpret the obtained experimental results. The results after energy-mass balance and evaluation demonstrated that profile-HSA-Hg^{2+} was more stable than profile-HSA-Cd-NCs. Also, the willingness of interaction between Hg^{2+} with the profile of HSA and profile-HSA-Cd-NCs was demonstrated. The obtained results after "energy-mass" balances depicted that HgG2 takes more stability in comparison with the appropriate species subsequent to removal of Hg^{2+} from profile-HSA-Hg^{2+} structure. Finally, an acceptable corroboration between experimental and theoretical obtained results was reported.

CRediT authorship contribution statement

Azarmidokht Sheini: Funding acquisition, Supervision, Writing - review & editing. **Avat(Arman) Taherpour:** Software. **Sakineh Farajmand-Amirabadi:** Investigation, Writing - original draft, Writing - review & editing. **Fatemeh Karampour:** Funding acquisition, Writing - review & editing. **Maryam Maghsudi:** Conceptualization, Data curation, Formal analysis, Funding acquisition, Investigation, Methodology, Project administration, Resources, Supervision, Validation, Visualization, Writing - original draft, Writing - review & editing. **Nadereh Rahbar:** Writing - review & editing.

Declaration of Competing Interest

The authors declare that they have no known competing financial interests or personal relationships that could have appeared to influence the work reported in this paper.

Acknowledgements

Financial support from the Ahvaz Jundishapur University of Medical Sciences and Shohadaye Hoveizeh University of Technology, Susangerd are gratefully acknowledged.

References

[1] A. Iqbal, K. Iqbal, L. Xu, B. Li, D. Gong, X. Liu, Y. Guo, W. Liu, W. Qin, H. Guo, Sens. Actuat. B 255 (2018) 1130, https://doi.org/10.1016/j.snb.2017.08.130.
[2] M. Wang, D.Q. Zhang, G.X. Zhang, Y.L. Tang, S. Wang, D.B. Zhu, Anal. Chem. 80 (2008) 6443, https://doi.org/10.1039/B921610C.
[3] J.W. Hong, W.L. Hemme, G.E. Keller, M.T. Rinke, G.C. Bazan, Adv. Mater. 18 (2006) 878, https://doi.org/10.1002/adma.200501605.
[4] P. Holmes, K.A.F. James, L.S. Levy, Sci. Total Environ. 408 (2009) 171.
[5] D.J. Yang, S. Shi, T.M. Yao, L.N. Ji, Biometals 25 (2012) 361, https://doi.org/10.1007/s10534-011-9505-7.
[6] P.B. Tchounwou, W.K. Ayensu, N. Ninashvili, D. Sutton, Environ. Toxicol. 18 (2003) 149, https://doi.org/10.1002/tox.10116.
[7] E. Hg, https://www.epa.gov/ground-water-and-drinking-water/national-primary-drinking-water-regulations#Inorganic (accessed December 25, 2019).
[8] J. Hirrlinger, R. Dringen, Brain Res. Rev. 63 (2010) 177, https://doi.org/10.1016/j.brainresrev.2009.10.003.

[9] I. Rahman, W. MacNee, Free Radical Biol. Med. 28 (2000) 1405, https://doi.org/10.1016/S0891-5849(00)00215-X.
[10] (a) X.F. Wang, M.S. Cynader, J. Neurosci. 21 (2001) 3322, https://doi.org/10.1523/JNEUROSCI.21-10-03322.2001;
(b) J. Liu, H.C. Yeo, E. Overvik-Douki, T. Hagen, S.J. Doniger, D.W. Chu, G.A. Brook, B.N. Ames, J. Appl. Physiol. 89 (2000) 21, https://doi.org/10.1152/jappl.2000.89.1.21.
[11] C.D. Geary, I. Zudans, A.V. Goponenko, S.A. Asher, S.G. Weber, Anal. Chem. 77 (2005) 185, https://doi.org/10.1021/ac048616k.
[12] R. Shunmugam, G.J. Gabriel, C.E. Smith, K.A. Aamer, G.N. Tew, Chem. – A European J. 14 (2008) 3904, https://doi.org/10.1002/chem.200701895.
[13] I. Chakraborty, T. Pradeep, Chem. Rev. 117 (2017) 8208, https://doi.org/10.1021/acs.chemrev.6b00769.
[14] H.T. Sun, S. Yoshio, Sci. Technol. Adv. Mater. 15 (2014), https://doi.org/10.1088/1468-6996/15/1/014205 014205.
[15] J.P. Xie, Y.G. Zheng, J.Y.J. Ying, J. Am. Chem. Soc. 131 (2009) 888, https://doi.org/10.1021/ja806804u.
[16] H.W. Li, Y. Yue, T.Y. Liu, D. Li, Y. Wu, J. Phys. Chem. C 117 (2013) 16159, https://doi.org/10.1021/jp403466b.
[17] M. B. Dickerson, K. H. Sandhage and R. R. Naik, Chemical Reviews, 2008, 108, 4935. DOI: 10.1021/cr8002328. Epub 2008 Oct 31.
[18] P.L. Xavier, K. Chaudhari, A. Baksi, T. Pradeep, Nano Rev. 3 (2012) 14767, https://doi.org/10.3402/nano.v3i0.14767.
[19] J.M. Slocik, D.W. Wright, Biomacromolecules 4 (2003) 1135, https://doi.org/10.1021/bm034003q.
[20] J.T. Petty, J. Zheng, N.V. Hud, R.M. Dickson, J. Am. Chem. Soc. 126 (2004) 5207, https://doi.org/10.1021/ja031931o.
[21] D.M. Chevrier, A. Chatt, P.J. Zhang, Nanophoton 6 (2012), https://doi.org/10.1117/1.JNP.6.064504 064504.
[22] A. Gupta, A. Chaudhary, P. Mehta, C. Dwivedi, S. Khan, N.C. Verma, C.K. Nandi, Chem. Commun. 51 (2015) 10750, https://doi.org/10.1039/C5CC03019F.
[23] Y.L. Wang, J.J. Chen, J. Irudayaraj, ACS Nano 5 (2011) 9718, https://doi.org/10.1021/nn2032177.
[24] Y. Shichibu, Y. Negishi, H. Tsunoyama, M. Kanehara, T. Teranishi, T. Tsukuda, Small 3 (2007) 835, https://doi.org/10.1002/smll.200600611.
[25] N. Goswami, A. Baksi, A. Giri, P.L. Xavier, G. Basu, T. Pradeep, S.K. Pal, Nanoscale 2014 (1848) 6, https://doi.org/10.1039/C3NR05784D.
[26] X. Le Guével, B. Hötzer, G. Jung, K. Hollemeyer, V. Trouillet, M. Schneider, J. Phys. Chem. C 115 (2011) 10955, https://doi.org/10.1021/jp111820b.
[27] M. Sarparast, A. Noori, H. Ilkhani, S.Z. Bathaie, M.F. El-Kady, L.J. Wang, H. Pham, K.L. Marsh, R.B. Kaner, M.F. Mousavi, Nano Res. 9 (2016) 3229, https://doi.org/10.1007/s12274-017-1633-0.
[28] M. Walter, J. Akola, O. Lopez-Acevedo, P.D. Jadzinsky, G. Calero, C.J. Ackerson, R.L. Whetten, H. Grönbeck, H. Häkkinen, PNAS 105 (2008) 9157, https://doi.org/10.1073/pnas.0801001105.
[29] N.J. Greenfield, Nat. Protoc. 1 (2006) 2876, https://doi.org/10.1038/nprot.2006.202.
[30] G. Wang, Y. Lu, H. Hou, Y. Liu, RSC Adv. 7 (2017) 9393, https://doi.org/10.1039/C6RA26089F.
[31] J. Liu, X. Yan, Y. Yue, Sh. Zhao, Luminescence 33 (2017) 104, https://doi.org/10.1002/bio.3378.
[32] A. Baksi, P.L. Xavier, K. Chaudhari, N. Goswami, S.K. Pal, T. Pradeep, Nanoscale 2013 (2009) 5, https://doi.org/10.1039/C2NR33180B.
[33] Y. Xu, J. Sherwood, Y. Qin, D. Crowley, M. Bonizzoni, Y.P. Bao, Nanoscale 6 (2014) 1515, https://doi.org/10.1039/C3NR06040C.
[34] A.A. Kamnev, L.A. Dykman, P.A. Tarantilis, M.G. Polissiou, Biosci. Rep. 22 (2002) 541, https://doi.org/10.1023/A:1022077920527.
[35] J.A. Seelenbinder, Ch.W. Brown, Ph. Pivarnik, A.G. Rand, Anal. Chem. 1999 (1963) 71, https://doi.org/10.1021/ac981170l.
[36] D.K. Sahu, P. Sarkar, D. Singha, K. Sahu, RSC Adv. 9 (2019) 39405, https://doi.org/10.1039/C9RA06774D.
[37] N. Goswami, K. Zheng, J. Xie, Nanoscale 6 (2014) 13328, https://doi.org/10.1039/C4NR04561K.
[38] R. W. Woody, Theory of Circular Dichroism of Proteins, in Circular dichroism and conformational analysis of biomolecules, New York. Fasman, G.D.(E.D), 1996.
[39] J.A. Ho, H.-C.H. Chang, W.T. Su, Anal. Chem. 84 (2012) 3246, https://doi.org/10.1021/ac203362g.
[40] X. Wang, Y. Yue, Y. Zhang, Z.H. Wang, J. Liu, Q. Tang, J. Mol. Struct. 1197 (2019) 210, https://doi.org/10.1016/j.molstruc.2019.07.061.
[41] Y. Yue, Z.H. Wang, Z.H. Wang, Y. Zhang, J. Liu, J. Mol. Struct. 1169 (2018) 75, https://doi.org/10.1016/j.molstruc.2018.05.060.
[42] J. Chen, J. Pan, Sh. Chen, Chem. Commun. 53 (2017) 10224, https://doi.org/10.1039/C7CC05445A.
[43] H.-C.H. Chang, Y.-F. Chang, N.-C.H. Fan, J.A. Ho, ACS Appl. Mater. Interf. 6 (2014) 18824, https://doi.org/10.1021/am504546f.
[44] D. Sahu, P. Mohapatra, S.K. Swain, J. Photochem. Photobiol. A 386 (2020), https://doi.org/10.1016/j.jphotochem.2019.112098 112098.
[45] M. Guo, J. Chi, Y. Li, G.I.N. Waterhouse, Sh. Ai, J. Hou, X. Li, Microchim. Acta 187 (2020) 534, https://doi.org/10.1007/s00604-020-04508-z.
[46] B.B. RasulKhan, P. Periakaruppan, S.K. Ponnaiah, G. Venkatachalam, B. Jeyaprabha, J. Cluster Sci. 32 (2021) 135, https://doi.org/10.1007/s10876-020-01770-2.
[47] H. Liu, X. Gao, X. Zhuang, Ch. Tian, Zh. Wang, Y. Li, A.L. Rogach, Analyst 144 (2019) 4425, https://doi.org/10.1039/C9AN00667B.
[48] Z. Suo, X. Hou, Z. Hu, Y. Liu, F. Xing, L. Feng, Microchim. Acta 186 (2019) 799, https://doi.org/10.1007/s00604-019-3919-2.
[49] L. Wang, T. Yao, S. Shi, Y. Cao, W. Sun, Sci. Rep. 4 (2014) 5320, https://doi.org/10.1038/srep05320.
[50] Z. Amouzegar, A. Afkhami, T. Madrakian, Microchim. Acta (2019) 186, https://doi.org/10.1007/s00604-019-3310-3.
[51] J. Zhu, T. Xia, Y. Cui, Y. Yang, G. Qian, J. Solid State Chem. 270 (2019) 317, https://doi.org/10.1016/j.jssc.2018.11.032.
[52] Y. Qiu, J. Huang, L. Jia, Int. J. Analyt. Chem. 1 (2018) ID 1979684, https://doi.org/10.1155/2018/1979684.
[53] Y. Bu, G. Zhu, S. Li, R. Qi, G. Bhave, D. Zhang, R. Han, D. Sun, X. Liu, Z. Hu, X. Liu, ACS Appl. Nano Mater. 1 (2018) 410, https://doi.org/10.1021/acsanm.7b00290.
[54] Y. Wang, X. Liu, M. Wang, X. Wang, W. Ma, J. Li, Sens. Actuat. B 329 (2021), https://doi.org/10.1016/j.snb.2020.129115 129115.
[55] Spatran '10-Quantum Mechanics Program: V2.0.3 Wavefunction Inc., USA, 2016.
[56] E. V. Anslyn and D. A. Dougherty, Modern Physical Organic Chemistry, University Science Books, Science, 2006.
[57] B. Meloun, L. Morávek, V. Kostka, FEBS Lett. 58 (1975) 134, https://doi.org/10.1016/0014-5793(75)80242-0.